LIU, Y., WANG, S., XIE, Y., FERNANDEZ, C., QIU, J. and ZHANG, Y. 2022. A novel adaptive H-infinity filtering method for the accurate SOC estimation of lithium-ion batteries based on optimal forgetting factor selection. *International journal of circuit theory and applications* [online], 50(10), pages 3372-3386. Available from: https://doi.org/10.1002/cta.3339

A novel adaptive H-infinity filtering method for the accurate SOC estimation of lithium-ion batteries based on optimal forgetting factor selection.

LIU, Y., WANG, S., XIE, Y., FERNANDEZ, C., QIU, J. and ZHANG, Y.

2022

A novel adaptive H-infinity filtering method for the accurate SOC estimation of lithium-ion batteries based on optimal forgetting factor selection

Yuyang Liu [a], Shunli Wang [a*], Yanxin Xie [a], Carlos Fernandez[b], Jingsong Qiu[a], Yixing Zhang[a]

[a]School of Information Engineering, Southwest University of Science and Technology, Mianyang 621010, China;

[b]School of Pharmacy and Life Sciences, Robert Gordon University, Aberdeen AB10-7GJ, UK.

Abstract: Accurate estimation of the state of charge (SOC) of lithium-ion batteries is quite crucial to battery safety monitoring and efficient use of energy, to improve the accuracy of lithium-ion battery SOC estimation under complicated working conditions, the research object of this study is the ternary lithium-ion battery, the forgetting factor recursive least square (FFRLS) method optimized by particle swarm optimization (PSO), and adaptive H-infinity filter (HIF) algorithm are adopted to estimate battery SOC. The PSO algorithm is improved with dynamic inertia weight to optimize the forgetting factor to solve the contradiction between FFRLS convergence speed and anti-noise ability. The noise covariance matrixes of the HIF are improved to realize adaptive correction function and improve the accuracy of SOC estimation. To verify the rationality of the joint algorithm, a second-order Thevenin model is established to estimate the SOC under three complex operating conditions. The experimental results show that the absolute value of the maximum estimation error of the improved algorithm under the three working conditions is 0.0192, 0.0131 and 0.0111 respectively, which proves that the improved algorithm has high accuracy, and offers a theoretical basis for the safe and efficient operation of the battery management system.

Keywords: Lithium-ion battery; Thevenin model; Forgetting factor recursive least square; Particle swarm optimization; H-infinity filter; State of charge

1 Introduction

With the rapid development of the emerging intelligent industry, the pollution problem facing the world has become more and more severe[1-4] at present. The energy crisis caused by excessive energy consumption has attracted widespread attention from all countries in the world[5-7]. Therefore, all countries are committed to the development and research of new energy sources to meet the needs of huge Energy demand and alleviate environmental pollution problems. Lithium-ion batteries have been widely used and developed in the field of new energy due to their advantages of high energy density, long life, lightweight and convenient portability[8-11]. To meet work requirements, lithium-ion batteries are often used in series and parallel groups. With the in-depth application of lithium-ion batteries in the field of new energy vehicles, its safety and reliability have been severely tested, due to individual differences in batteries, over-charging, over-discharging and overheating often occur during use. To solve the above problems, battery management system (BMS) came into being[12-14]. BMS can detect the physical parameters of the lithium-ion battery and estimate SOC. Lithium-ion battery SOC is the core parameter of BMS, it can characterize the remaining power of the battery[15]. The accurate estimation can make the BMS more accurately judge the timing of equilibrium, and the accuracy of the SOC estimation much depends on the accurate establishment of the battery equivalent model[16-19]. Therefore, how establishing an equivalent model for the operating characteristics of a lithium-ion battery and using a correct and appropriate algorithm to estimate the battery SOC is the key to establishing a battery management system and is of great significance to improving battery efficiency.

Currently, the commonly used battery models include electrochemical models, neural network models, and equivalent circuit models[20, 21]. After establishing an accurate equivalent model and performing parameter identification, relevant algorithms can be used to estimate the SOC[22, 23]. Commonly used SOC estimation methods include the ampere-hour integration method, Kalman filter and its extended algorithm, neural network method and so on[24, 25]. Duan et al. use extended Kalman filter (EKF) to update model parameters, and adaptive unscented Kalman filter (AUKF) to predict battery SOC, the results prove that EKF-AUKF has high estimation accuracy[26]. Yang et at. proposed a long short-term memory (LSTM)-cyclic neural network to simulate complex battery behavior at different temperatures and estimate the battery SOC based on voltage, current, and temperature variables. Combined with UKF to filter out the noise and further reduce estimation errors[27, 28]. Hu et al. adopted a novel SOC estimation method for series-connected battery packs based on the fuzzy adaptive federated filtering, it combines the SOC estimation value of the cell average model and the standard deviation of the SOC estimation with the fuzzy system to determine their fusion weight. The main filter adaptively adjusts the information distribution coefficient according to the estimation accuracy of the local filter to improve reliability[29, 30].

To perform higher-precision online parameter identification and accurate battery SOC estimation, this research constructed a second-order Thevenin equivalent circuit model and proposed an improved particle swarm optimization forgetting factor least square method combined with adaptive HIF algorithm for SOC estimation method, through the hybrid pulse power characterization (HPPC), dynamic stress test (DST) and Beijing Bus dynamic stress test (BBDST) working conditions for experimental analysis to verify the effectiveness of the improved algorithm.

Nomenclature			
		R_2	electrochemical polarization resistance (Ω)
Acronyms		C_2	electrochemical polarization capacitance (F)
SOC	state of charge	Q_v	rated battery capacity (Ah)
RLS	recursive least square	η	Coulomb efficiency
FFRLS	forgetting factor recursive least square	τ_1	time constant
PSO	Particle swarm optimization	τ_2	time constant
IPSO	improved particle swarm optimization	$w(k)$	process noise
HIF	H-infinity filter	$v(k)$	measurement noise
AHIF	adaptive H-infinity filter	$\varphi(k)$	observation vector
BMS	battery management system	$\theta(k)$	parameter vector
EKF	extended Kalman filter	$e(k)$	observation noise vector
AUKF	adaptive unscented Kalman filter	$J(\theta)$	objective function
LSTM	long short-term memory	λ	forgetting factor in FFRLS
HPPC	hybrid pulse power characterization	V_{id}	velocity of the particle
DST	dynamic stress test	P_i	individual extreme value of the particle
BBDST	Beijing Bus dynamic stress test	P_g	group extreme value of the population
RC	resistance-capacitance	c_1	acceleration factor
Ah	ampere-hour	c_2	acceleration factor
OCV	open circuit voltage	r_1	random number
MAE	Mean Absolute Error	r_2	random number
RMSE	Root Mean Square Error	ω_s	initial inertia weight
List of symbols & parameters		ω_e	maximum number inertia weight
		J	cost function
U_{OC}	open circuit voltage (V)	P_0	initial error covariance matrix
U_L	terminal voltage (V)	P_0	initial error covariance matrix
E	ideal voltage source	θ	performance boundary
R_0	ohmic internal resistance (Ω)	K_k	filter gain matrix
R_1	polarization resistance (Ω)	S_k	third-order positive definite matrix
C_1	polarization capacitance (F)	δ	forgetting factor in AHIF

2 Theoretical analysis

2.1 Equivalent circuit modeling

The accurate estimation of the lithium-ion battery state is based on an accurate circuit equivalent model. Among the commonly used circuit models, the Rint model has a relatively simple structure, including only an ideal voltage source *Uoc* and internal resistance R_0, and the model accuracy is low[31, 32]; Thevenin model adds an RC parallel circuit based on the Rint model to characterize the polarization effect of the battery [33]. This model is also simple and can meet the simulation requirements, but it cannot accurately describe the dynamic characteristics of the battery[34]. To solve this problem and comprehensively consider the accuracy and simplicity of battery modeling, this research adds an RC parallel circuit to the first-order Thevenin model to obtain the second-order Thevenin model, as shown in Figure. 1.

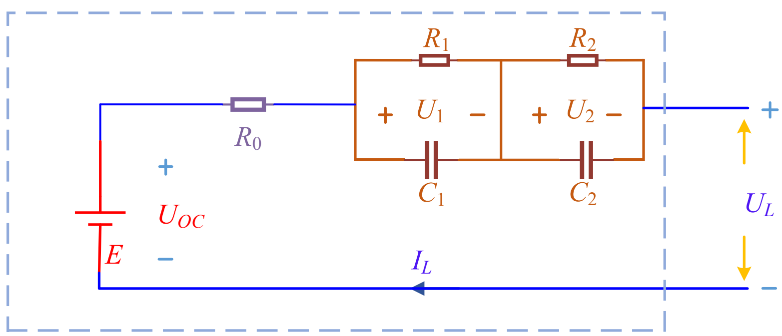

Figure. 1 Second-order Thevenin model

In Figure. 1, U_{OC} represents the open circuit voltage of the battery, U_L represents the terminal voltage after the battery is connected to an external circuit, E is the ideal voltage source, R_0 is the ohmic internal resistance, which represents the transient response of the charging and discharging voltage, and R_1 is the polarization resistance of the battery; C_1 is the polarization capacitance, which represents the change in the polarization voltage U_1 caused by the load current I_L. The parallel circuit of R_1 and C_1 describes the polarization reaction of the battery, and this process characterizes the rapid reaction of the electrode to the battery. R_2 and C_2 are the electrochemical polarization resistance and capacitance, respectively, which characterize the slow reaction of the electrode to the battery. The improved second-order Thevenin model can better describe the dynamic characteristics of the lithium-ion battery during charging and discharging. The circuit equation can be obtained from Kirchhoff's law：

$$\begin{cases} U_L(t)=U_{oc}(t)-U_0(t)-U_1(t)-U_2(t) \\ I_L=C_1\dfrac{dU_1}{dt}+\dfrac{U_1}{R_1}=C_2\dfrac{dU_2}{dt}+\dfrac{U_2}{R_2} \\ U_{\text{oc}}=f[SOC(t)] \\ SOC(t)=SOC(0)-\eta\int_0^t\dfrac{i}{Q_v}dt \\ U_0=R_0I_L \end{cases} \tag{1}$$

In Equation (1), $SOC(0)$ is the initial SOC value, $SOC(\mathrm{t})$ is the SOC value after t time has elapsed, Q_v represents the rated battery capacity, and η represents the Coulomb efficiency. The following equation can be obtained after discretizing Equation (1).

$$\begin{cases} \begin{bmatrix} SOC(k+1) \\ U_1(k+1) \\ U_2(k+1) \end{bmatrix}=\begin{pmatrix} 1 & 0 & 0 \\ 0 & e^{\frac{-T}{\tau_1}} & 0 \\ 0 & 0 & e^{\frac{-T}{\tau_2}} \end{pmatrix}\begin{pmatrix} SOC(k) \\ U_1(k) \\ U_2(k) \end{pmatrix}+\left[\dfrac{-\eta T}{Q_v} \; R_1\left(1-e^{\frac{-\mathrm{T}}{\tau_1}}\right) \; R_2\left(1-e^{\frac{-\mathrm{T}}{\tau_2}}\right)\right]^{\mathrm{T}} I(k)+w(k) \\ U_L(k)=\left(\dfrac{\partial U_{oc}}{\partial SOC} \quad -1 \quad -1\right)\left[SOC(k) \quad U_1(k) \quad U_2(k)\right]^{\mathrm{T}}-R_0I(k)+v(k) \end{cases} \tag{2}$$

In Equation (2), T is the sampling period; $\tau_1=R_1*C_1$; $\tau_2=R_2*C_2$; $w(k)$ and $v(k)$ are the process noise and measurement noise at time k, respectively.

2.2 Improved optimal forgetting factor least square method

Recursive least square (RLS) has the characteristics of easy understanding and fast convergence and has been widely used in the field of system identification[35, 36]. However, due to the phenomenon of "filter saturation" in the recursive least square method, that is, as the number of algorithm data iterations increases, the values of gain K and P will become smaller and smaller. This makes the algorithm's ability to correct data gradually weaker, and the degree of data saturation becomes larger and larger, which eventually leads to larger and larger parameter identification errors. Therefore, the forgetting factor is considered to be added in the identification of the least squares method to improve the online estimation ability of the RLS algorithm. The mathematical description expression of the least square method is shown in Equation (3).

$$y(k)=\varphi(k)\theta^T+e(k) \tag{3}$$

Wherein, $\varphi(k)$ is the observation vector; $\theta(k)$ is the parameter vector to be estimated; $e(k)$ is the observation noise vector.

The objective function $J(\theta)$ is taken in RLS, the purpose of the algorithm is to find $\hat{\theta}$, when $\theta=\hat{\theta}$, $J(\theta)$ takes the minimum value. The objective function and estimated parameter values of the system are shown in Equation (4).

$$\begin{cases} J\left(\hat{\theta}\right) = [y(k) - \varphi(k)\hat{\theta}(k)]^{\mathrm{T}}[y(k) - \varphi(k)\hat{\theta}(k)] \\ \hat{\theta} = [\varphi(k)\varphi(k)^{\mathrm{T}}]^{-1}\varphi(k)y(k) \end{cases} \tag{4}$$

In the actual simulation calculation, it is necessary to continuously input and output the latest experimental data, and improve the accuracy of parameter estimation in the continuous iterative process until a satisfactory accuracy is achieved. After introducing the forgetting factor λ ($0 < \lambda < 1$), the specific calculation process is shown in Equation (5).

$$\begin{cases} \hat{\theta}(k+1) = \hat{\theta}(k) + K(k+1)[y(k+1) - \phi^{T}(k+1)\hat{\theta}(k)] \\ K(k+1) = P(k+1)\phi(k+1)[\phi^{T}(k+1)P(k)\phi(k+1) + \lambda]^{-1} \\ P(k+1) = \lambda^{-1}[I - K(k+1)\phi^{T}(k+1)]P(k) \end{cases} \tag{5}$$

Wherein, λ generally has a value range of 0.95-1, $\hat{\theta}(k)$ is the estimated value of the parameter at time k, $\phi^{\mathrm{T}}(k+1)\hat{\theta}(k)$ is the calculated value of the system observation at time k+1, and wherein $\phi^{\mathrm{T}}(k+1)$ is the observed value matrix of voltage and current. $y(k+1)$ is the actual observed value at time k+1. In each iteration, the algorithm uses the difference between the system observation calculation value and the actual observation value, and the gain K to correct the final estimated value. However, when λ is a fixed value, there is a contradiction between the convergence speed and the anti-noise ability. A small value of λ will lower the anti-noise ability and result in low identification accuracy; while a large value of λ will result in a slower convergence speed. Therefore, this research employs the particle swarm optimization algorithm to optimize the forgetting factor in real-time, finds the optimal λ in each iteration of the algorithm, dynamically adjusts the value of λ, and improves the identification accuracy of the forgetting factor least square method. In the particle swarm optimization algorithm, the particle velocity and position update equations are shown in Equation (6).

$$\begin{cases} V_{id}^{k+1} = \omega V_{id}^{k} + c_1 r_1\left(P_{id}^{k} - X_{id}^{k}\right) + c_2 r_2\left(P_{gd}^{k} - X_{gd}^{k}\right) \\ X_{id}^{k+1} = X_{id}^{k} + V_{id}^{k+1} \end{cases} \tag{6}$$

In Equation (6), ω is the inertia weight; $d = 1, 2, \cdots, D$, D is the number of particles; $i = 1, 2, \cdots, n$; k is the current iteration number; V_{id} is the velocity of the particle; P_i is the individual extreme value of the particle, P_g is the group extreme value of the population;c_1 and c_2 are non-negative constants which are called acceleration factors; r_1 and r_2 are random numbers distributed in the interval. In this research, the actual terminal voltage and the estimated terminal voltage are taken as the fitness function, as shown in Equation (7).

$$f=\left|U(k)-U_{OC}(k)-\varphi^{\mathrm{T}}(k)\hat{\theta}(k-1)\right| \tag{7}$$

Wherein, $U(k)$ represents the actual terminal voltage, $\varphi^{\mathrm{T}}(k)\hat{\theta}(k-1)$ is the system observation value at time k.

The inertia weight ω reflects the ability of the particle to inherit the previous velocity. A larger ω is conducive to the global search and a smaller ω is more conducive to the local search. To better balance the global and local search capabilities of the particle swarm optimization algorithm, the inertia weight ω is improved, as shown in the following equation.

$$(k)=\omega_s-(\quad {}_s-\omega_e)\left(\frac{k}{T_{\max}}\right)^2 \tag{8}$$

In Equation (8), ω_s is the initial inertia weight; ω_e is the inertia weight when the iteration reaches the maximum number of times; k is the current iteration number; $T_{\max}$ is the maximum iteration number. In general, the algorithm performance is best when the inertia weight ω_s = 0.9 and ω_e = 0.4. As the iteration progresses, the inertia weight decreases linearly from 0.9 to 0.4, which ensures that the optimization algorithm has a strong global search ability in the early stage, and a more accurate local search can be performed in the later stage of the iteration. The flow chart of the particle swarm optimization algorithm is shown in the figure below.

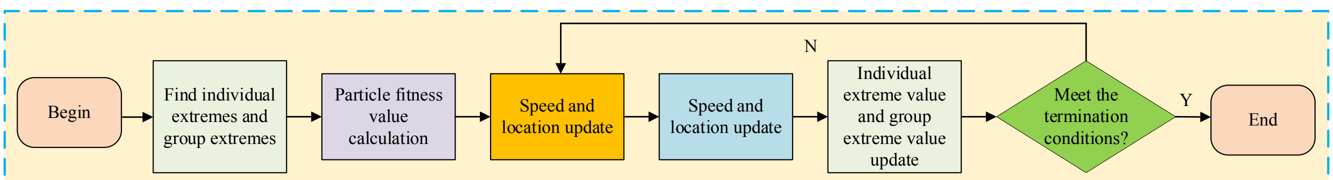

Figure. 2 Flowchart of particle swarm optimization algorithm

In Figure. 2, the particle speed and position are randomly initialized by initialization; the particle fitness value is calculated according to Equation (7); the individual extremum and the group extremum are determined according to the initial particle fitness value; the particle speed and position are updated by Equation (6); The individual extreme value and the group extreme value are updated according to the fitness value of the particles in the new population.

2.3 Adaptive HIF algorithm

From the discrete system Equation (2), the following equation can be derived.

$$\begin{cases} X_{k+1} = A_k X_k + B_k u_k + w_k \\ Y_k = C_k x_k + D_k u_k + v_k \end{cases} \tag{9}$$

In Equation (9), x_k is the state variable; u_k is the system input; A_k is the state transition matrix, which predicts the system variables; B_k is the system control input matrix; C_k and D_k are the system observation matrices, driving the forecasting system observations; w_k and v_k are independent Gaussian white noises. Combined with the state space expression of the battery, the expressions of A_k、B_k、C_k and D_k can be obtained, as shown in Equation (10).

$$\begin{cases} A_k = \begin{pmatrix} 1 & 0 & 0 \\ 0 & e^{\frac{-T}{\tau_1}} & 0 \\ 0 & 0 & e^{\frac{-T}{\tau_2}} \end{pmatrix} \qquad B_k = \left[\frac{-\eta T}{Q_v} R_1 \left(1 - e^{\frac{-\mathrm{T}}{\tau_1}} \right) R_2 \left(1 - e^{\frac{-\mathrm{T}}{\tau_2}} \right) \right]^{\mathrm{T}} \\ C_k = \begin{pmatrix} \frac{\partial U_{oc}}{\partial SOC} & -1 & -1 \end{pmatrix} \qquad D_k = \left[-R_0 \right] \end{cases} \tag{10}$$

The HIF algorithm adopts the idea of game theory and introduces a cost function J[37], as shown in Equation (11).

$$J_1 = \frac{\sum_{k=0}^{N-1} \left\| x_k - \hat{X}_k \right\|_{S_k}^2}{\left\| x_0 - X_0 \right\|_{P_0^{-1}}^2 + \sum_{k=0}^{N-1} \left(\left\| w_k \right\|_{Q_k^{-1}}^2 + \left\| v_k \right\|_{R_k^{-1}}^2 \right)} \tag{11}$$

In Equation (11), x_0 and X_0 are the initial value and initial setting value of the state variable respectively; P_0 is the initial error covariance matrix; Q_k and R_k are the covariance matrix of w_k and v_k. The goal of HIF is to find an estimated value of $\hat{X}_k$ such that $x_k - \hat{X}_k$ takes the minimum value to obtain the best estimate[37, 38]. In practical applications, it is difficult to minimize it directly, therefore, an appropriate performance boundary θ is selected to satisfy the conditions in Equation (12).

$$J < \frac{1}{\theta} \tag{12}$$

Combining Equation (11) and Equation (12), the expression of the cost function J_1 can be obtained, as shown in Equation (13).

$$J_1 = -\frac{1}{\theta} \left\| x_0 - X_0 \right\|_{P_0^{-1}}^2 \sum_{k=0}^{N-1} \left[\left\| x_k - \hat{X}_k \right\|_{S_k}^2 - \frac{1}{\theta} \left(\left\| w_k \right\|_{Q_k^{-1}}^2 + \left\| v_k \right\|_{R_k^{-1}}^2 \right) \right] < 0 \tag{13}$$

Combining Equation (9) and Equation (13), the recurrence relationship of the HIF algorithm can be obtained as shown in the following equation.

$$\begin{cases} K_k = P_k\left[I-\theta S_k P_k + C_k^T R_k^{-1} C_k P_k\right]^{-1} C_k^T R_k^{-1} \\ X_{k+1} = A\hat{X}_k + Bu_k + K_k\left(y_k - \hat{y}_k\right) \\ P_{k+1} = AP_k\left[I-\theta S_k P_k + C_k^T R_k^{-1} C_k P_k\right]^{-1} A^{\mathrm{T}} + Q_k \end{cases} \tag{14}$$

In Equation (14), K_k is the filter gain matrix; S_k is a third-order positive definite matrix, which is set by the importance of each state. The noise covariance matrixes Q_k and R_k in the HIF algorithm are both artificially set fixed values. To improve the estimation performance of the algorithm, Q_k and R_k are improved, and the noise covariance matrix is updated in real-time using measurement data, as shown in Equation (15).

$$\begin{cases} Q_k = \left(1-d_{k-1}\right)Q_{k-1} + d_{k-1}\left(K_k \tilde{y}_k \tilde{y}_k^{\mathrm{T}} K^{\mathrm{T}} + P_k - AP_{k-1}A^{\mathrm{T}}\right) \\ R_k = \left(1-d_{k-1}\right)R_{k-1} + d_{k-1}\left(\tilde{y}_k \tilde{y}_k^{\mathrm{T}} - CR_{k-1}C^{\mathrm{T}}\right) \\ \tilde{y}_k = U_{L|k} - C_k X_k - I_L R_0 \end{cases} \tag{15}$$

In Equation (15), $d_{k-1} = \frac{1-\delta}{1-\delta^{k}}$; δ is forgetting factor, $0<\delta<1$, $\delta = 0.96$. It can be seen from Equation (15) that the estimation accuracy of SOC can be improved and the correction function can be realized according to the real-time estimation of Q_k and R_k. The entire SOC estimation process is shown in Figure. 3, and the values of different parameters in experimental verification are shown in Table 1.

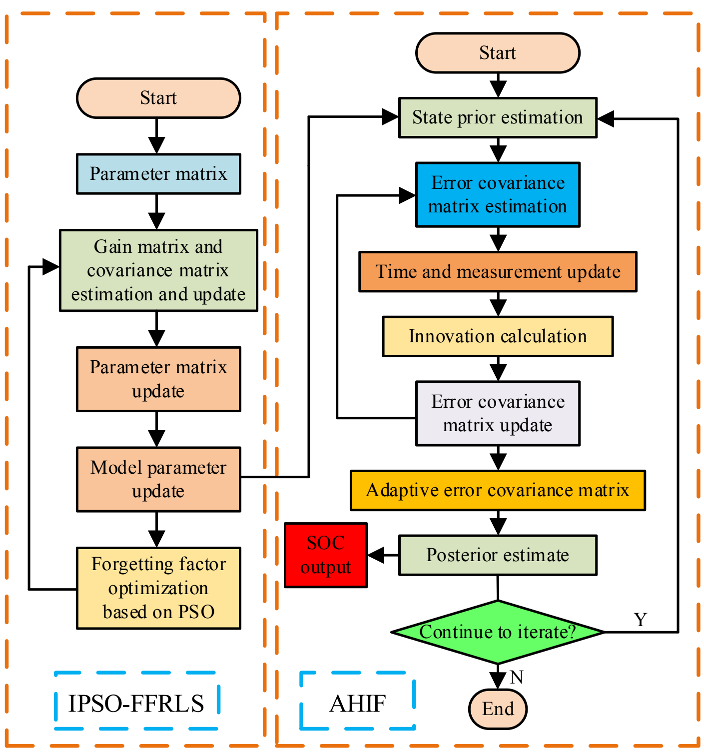

Figure. 3 Flowchart of the whole algorithm

Table 1. Values of different parameters

Algorithms	Parameters
FFRLS	$\lambda_0 = 0.98$
IPSO	$\lambda \in (0.95,1)$
HIF	$P = \begin{bmatrix} 1 & 0 & 0 \\ 0 & 1 & 0 \\ 0 & 0 & 1 \end{bmatrix}$
	$Q = 1 \times 10^{-8} \times \begin{bmatrix} 1 & 0 & 0 \\ 0 & 1 & 0 \\ 0 & 0 & 1 \end{bmatrix}$
	$R = 1 \times 10^{-3} \times \begin{bmatrix} 1 & 0 & 0 \\ 0 & 1 & 0 \\ 0 & 0 & 1 \end{bmatrix}$
AHIF	$\delta = 0.96$
	$S_k = \begin{bmatrix} 0.01 & 0 & 0 \\ 0 & 0.01 & 0 \\ 0 & 0 & 0.01 \end{bmatrix}$

3 Experimental analysis

The battery used in the experiment is a ternary lithium-ion battery with a rated capacity of 70Ah and an actual capacity of 68Ah. The battery charging and discharging equipment adopts the power battery module test system BTS750-200-100-4, and the thermostat is BTKS5-150C. Since the internal parameters of the battery change with temperature, this experiment was carried out under the condition of 25°C. The experimental platform is shown in Figure. 4.

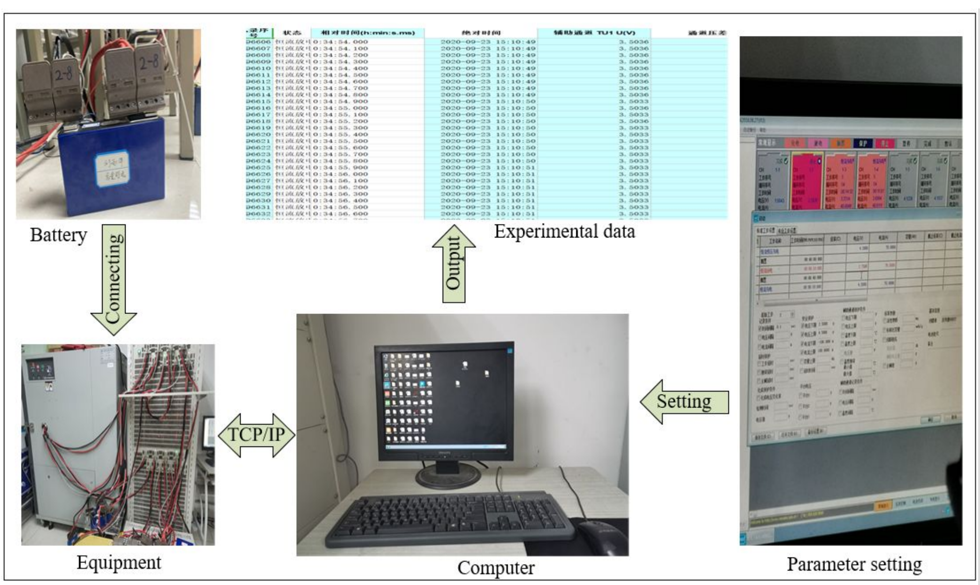

Figure. 4 Experimental platform

3.1 SOC-OCV fitting curve

Because of the good mapping relationship between battery SOC and OCV, in the process of online parameter identification of the battery based on the IPSO-FFRLS algorithm, it is necessary to obtain a more accurate SOC-OCV curve to avoid large observation errors. In this research, the HPPC test is employed to obtain the current and voltage data of the single battery, and the model is used to identify effective online parameters. The HPPC experiment steps are as follows:

① At first, the lithium-ion battery is charged as standard. After the end of charging, shelve it for 2h, where the charging current is set to 1C (68Ah), the charging voltage is set to 4.5V, and the cut-off condition is set to the current 3.4A.

② After the battery is fully charged, a current pulse experiment is conducted on the battery. It is discharged with a current of 1C for 10s firstly, then shelved for 40s, and then charged with a current of 1C for 10s. The purpose is to return the battery to the SOC value before discharge and complete a set of pulse charge and discharge experiments.

③ The battery is discharged with a current of 1C for 6 minutes (battery SOC is 90%), and then shelved for 1h. The cut-off condition is 3V.

④ Repeat step ② and step ③, discharge with 10% capacity for each cycle and record relevant data at SOC of 1, 0.9,..., 0 to provide data for the parameter identification.

The functional relationship of SOC-OCV is obtained from the HPPC test data as shown in Equation (16).

$$U_{OC} = 4.265 \times SOC^5 - 14.9 \times SOC^4 + 19.38 \times SOC^3 - 10.77 \times SOC^2 + 2.947 \times SOC + 3.251 \tag{16}$$

After comparing the fitting effect many times, it is found that the 5th-order polynomial avoids excessive fitting and the complexity of the processor under the premise of ensuring the fitting effect. Therefore, this research chooses the 5th-order polynomial to fit the SOC-OCV curve.

3.2 Analysis of parameter identification results

To verify the effectiveness of the IPSO-FFRLS algorithm, the online parameter identification of the model was performed with the RLS, FFRLS and IPSO-FFRLS algorithms. The parameter identification results are shown in the figure below.

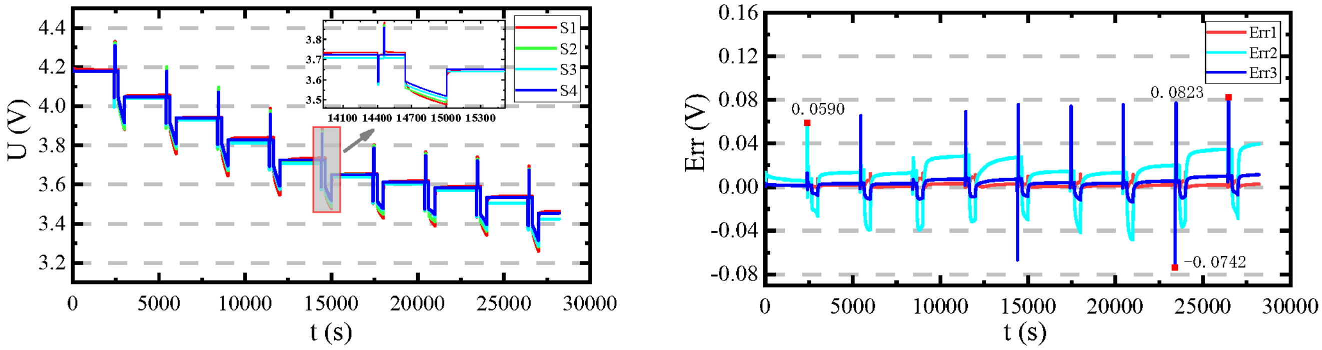

(a) Comparison of identification results of HPPC condition

(b) Comparison of identification errors

Figure. 5 Parameter identification results of HPPC condition

Figure. 5(a) shows the voltage comparison diagram of the parameter identification results of the three algorithms, wherein, S1 represents the actual voltage, S2 represents the analog voltage corresponding to the IPSO-FFRLS algorithm, S3 represents the analog voltage corresponding to the FFRLS algorithm, and S4 represents the RLS algorithm corresponding analog voltage. Figure. 5(b) shows the voltage error comparison diagram of the identification results of the three algorithms. Err1, Err2 and Err3 represent the voltage error curves corresponding to the IPSO-FFRLS, FFRLS and RLS algorithms, respectively. In this research, the fixed forgetting factor in FFRLS is 0.98, the value range of the forgetting factor set in the IPSO-FFRLS is 0.95-1. It can be seen from Figure. 5 (b) that among the three parameter identification methods, the voltage fluctuation range of the IPSO-FFRLS algorithm is the smallest, and the maximum voltage error does not exceed ±0.02V, which proves that the improved algorithm has better parameter identification effect and higher accuracy, can be used for state estimation later.

3.3 SOC estimation under complex working conditions

3.3.1 Analysis of experimental results under HPPC working conditions

In actual application scenarios, batteries are mostly in intermittent charging and discharging states. The HPPC test includes charging and discharging and shelving steps, which can better simulate the actual working state of the battery, so the HPPC working condition is used for experimental verification, the estimated effects of the fixed forgetting factor FFRLS algorithm and the IPSO-FFRLS algorithm are compared. In addition, the SOC estimation results of the EKF, HIF, AHIF algorithms are compared, as shown in Figure. 6.

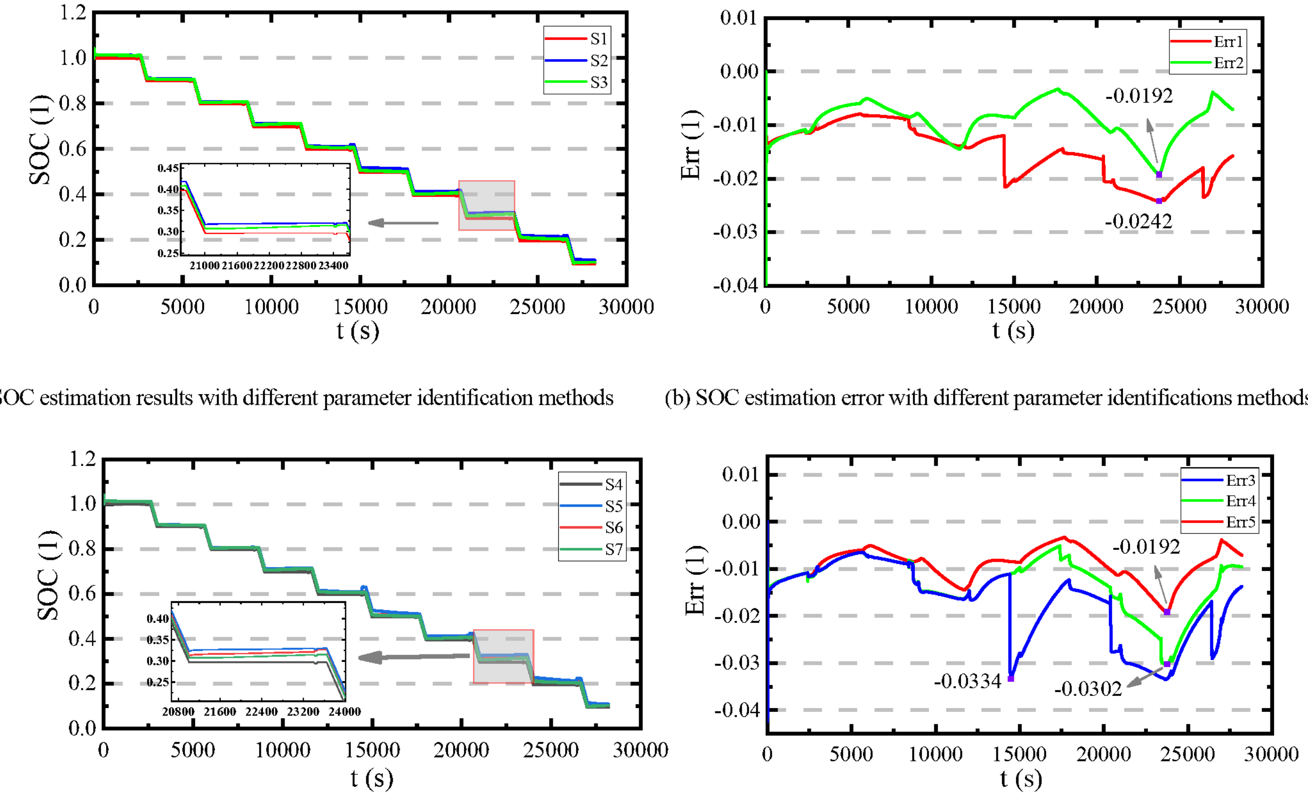

(a) SOC estimation results with different parameter identification methods (b) SOC estimation error with different parameter identifications methods

(c) SOC estimation results with different algorithms (d) SOC estimation error with different algorithms

Figure. 6 SOC estimation results and errors of HPPC condition

In Figure. 6, S1-S3 respectively represent the SOC reference value, the SOC estimated value based on fixed forgetting factor FFRLS and AHIF, and the SOC estimated value based on IPSO-FFRLS and AHIF. Err1-Err2 correspond to the estimated errors of S2-S3, respectively. S4-S7 respectively represent the SOC reference value, SOC estimation results of the EKF, HIF and AHIF algorithms. Err3-Err5 correspond to the estimated errors of S5-S7, respectively. It can be seen from Figure. 6(c) that the SOC estimation error of the IPSO-FFRLS algorithm is smaller than that based on the fixed forgetting factor FFRLS algorithm in almost the entire estimation process under HPPC working conditions, which shows that the parameter identification effect of IPSO-FFRLS algorithm is better. It can be seen from Fig. 6(d) that the errors of the three algorithms in the middle and latter stages of SOC estimation are relatively large, which is caused by the severe chemical reaction inside the battery at the end of discharge. The estimation error of the AHIF algorithm is significantly lower than that of other algorithms, the maximum absolute error is 0.0192, and it can also track the reference value better, which reflects the superiority of the proposed AHIF algorithm. To compare the SOC estimation results of the algorithms more intuitively, the Mean Absolute Error (MAE) and Root Mean Square Error (RMSE) of the estimation results are compared and analyzed, as shown in Table 2.

Table 2. Comparison of performance indicators of various algorithms under HPPC working conditions

Algorithms	MAE	RMSE
IPSO-EKF	1.708%	1.877%
IPSO-HIF	1.315%	1.428%
FFRLS-AHIF	1.511%	1.588%
IPSO-AHIF	0.919%	0.984%

3.3.2 Analysis of experimental results under DST working conditions

In practical applications, the current is also complex and changeable, often accompanied by sudden switching and stopping, which puts forward strict requirements on the dynamic performance of the battery, and also brings challenges to the stability of the algorithm. To verify the SOC estimation of the improved algorithm under more complex conditions, the improved algorithm is simulated and verified by dynamic test stress conditions. The verification result is shown in the figure below.

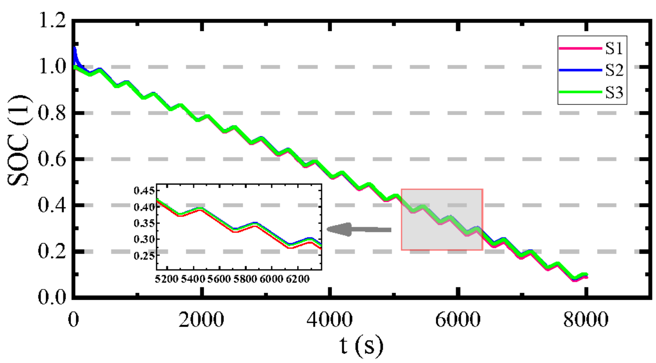

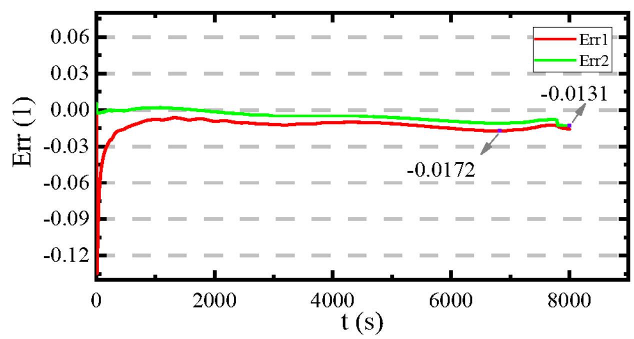

(a) SOC estimation results with different parameter identification methods (b) SOC estimation error with different parameter identifications methods

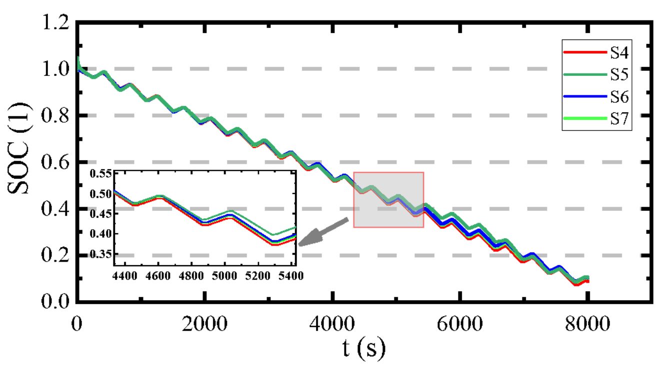

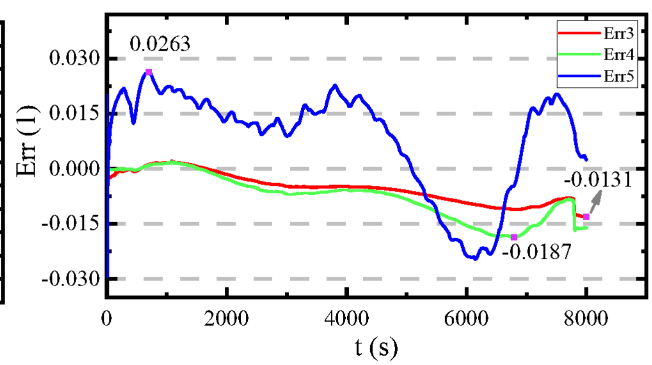

(c) SOC estimation results with different algorithms (d) SOC estimation error with different algorithms

Figure. 7 SOC estimation results and errors of DST condition

The legend in Figure. 7 is consistent with Figure. 6. It can be seen from Figure. 7(b) that the convergence time of the IPSO-FFRLS algorithm is significantly faster than the fixed forgetting factor FFRLS algorithm under DST working conditions, and the estimation accuracy of the IPSO-FFRLS algorithm is always higher. It indicates that under more complex conditions, the IPSO-FFRLS algorithm has a better parameter identification effect and faster convergence speed. It can be seen from

(c) SOC estimation results with different algorithms (d) SOC estimation error with different algorithms

Figure. 7(d) that under more complex conditions, the HIF and AHIF algorithms almost coincide with the actual SOC curve in the early stage of estimation, and the maximum estimation error of the two algorithms in the later stage is also within 0.02. It shows that the HIF algorithm has a better estimation effect under the uncertainty of the system model and external interference, in the case of severe chemical reaction in the later stage of discharge, the error fluctuation of the AHIF algorithm is smaller and more stable. The maximum absolute estimation error of the AHIF algorithm is 0.0131, and the estimation error interval is kept within ±0.014, which proves that the AHIF algorithm has strong estimation stability under more complicated working conditions. The MAE and RMSE of the estimation results under DST working conditions are shown in Table 3.

Table 3. Comparison of performance indicators of various algorithms under DST working conditions

Algorithms	MAE	RMSE
IPSO-EKF	1.512%	1.624%
IPSO-HIF	0.777%	0.963%
FFRLS-AHIF	1.335%	1.593%
IPSO-AHIF	0.548%	0.652%

3.3.3 Analysis of experimental results under BBDST working conditions

To further verify the estimated performance of the improved algorithm in the actual complex working conditions of the lithium-ion battery, the research refers to the Beijing Bus Dynamic Stress Test (BBDST) working condition to conduct a corresponding test on the battery. The BBDST working condition steps include starting, accelerating, sliding, braking, rapid acceleration and parking steps, which are the working conditions obtained by real data collection of Beijing buses, which can restore the actual working state of the lithium-ion battery. SOC estimation results are shown in

(c) SOC estimation results with different algorithms (d) SOC estimation error with different algorithms

Figure. 8.

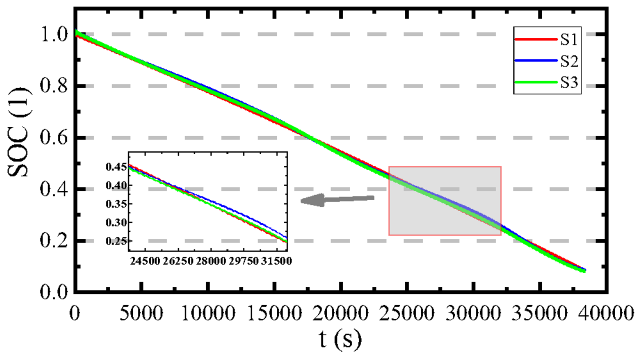

(a) SOC estimation results with different parameter identification methods

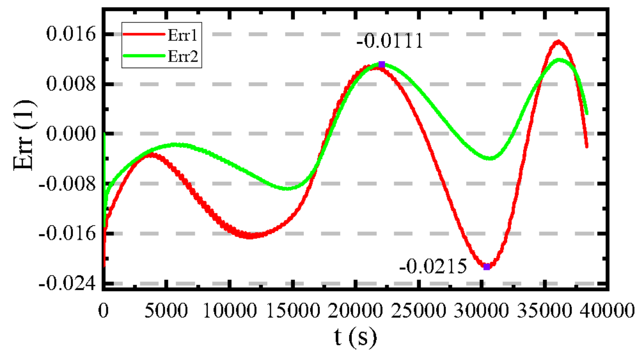

(b) SOC estimation error with different parameter identifications methods

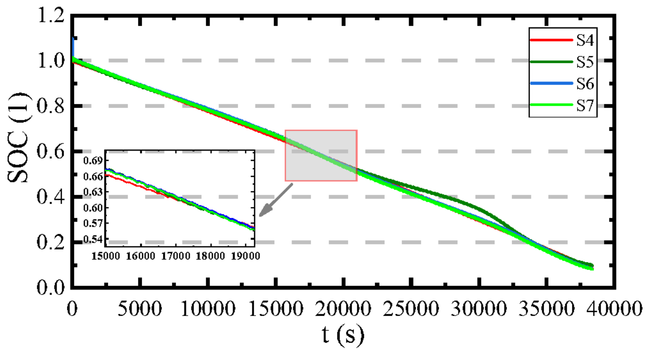

(c) SOC estimation results with different algorithms

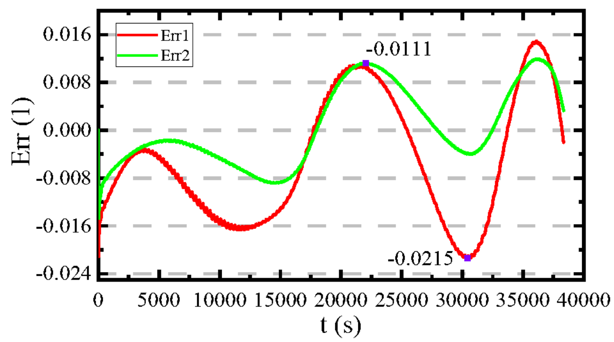

(d) SOC estimation error with different algorithms

Figure. 8 SOC estimation results and errors of BBDST condition

In

(c) SOC estimation results with different algorithms (d) SOC estimation error with different algorithms

Figure. 8(a), S1 represents the actual SOC curve, S2 represents the SOC curve estimated by the EKF algorithm, S3 represents the SOC curve estimated by the HIF algorithm, and S4 represents the SOC curve estimated by the AHIF algorithm. In

(c) SOC estimation results with different algorithms (d) SOC estimation error with different algorithms

Figure. 8(b), Err1-Err3 correspond to the estimation error of S2-S4 respectively. It can be seen from

(c) SOC estimation results with different algorithms (d) SOC estimation error with different algorithms

Figure. 8 that in the BBDST operating condition, which is more complex than the DST operating condition, there are more sudden changes in current, and the error of the EKF algorithm fluctuates greatly, while the HIF and AHIF algorithms are always in the whole SOC estimation process. In a more stable state, the maximum absolute estimation errors are 0.0122 and 0.0111, respectively, and the mean absolute errors of the HIF and AHIF algorithms are 0.0063 and 0.0057, which proves that the improved algorithm has higher estimation accuracy under complex working conditions.

The legend in Figure. 8 is consistent with Figure. 6. It can be seen from

(c) SOC estimation results with different algorithms (d) SOC estimation error with different algorithms

Figure. 8 that in the BBDST operating condition, which is more complex than the DST operating condition, there are more sudden changes in current, and the error of the EKF algorithm fluctuates greatly, while the HIF and AHIF algorithms remained stable in the whole SOC estimation process. In HIF algorithm, the process and measurement noise covariances are constant, but in the SOC estimation process, the noise covariance may change with the changes in operating conditions inside and around the battery. Therefore, AHIF algorithm which can dynamically adjust the noise covariance is proposed to estimate SOC. The maximum absolute estimation error of the AHIF algorithm is 0.111, which proves that the proposed AHIF algorithm still has the highest accuracy. The MAE and RMSE of the estimation results under BBDST working conditions are shown in Table 4.

Table 4. Comparison of performance indicators of various algorithms under BBDST working conditions

Algorithms	MAE	RMSE
IPSO-EKF	1.633%	1.755%
IPSO-HIF	0.635%	0.716%
FFRLS-AHIF	1.014%	1.145%
IPSO-AHIF	0.571%	0.660%

Combining the comparison diagrams of several algorithms under the three working conditions, the IPSO-FFRLS algorithm can identify battery parameters more accurately, and has a faster convergence time than FFRLS algorithm with a fixed forgetting factor. It can be seen that the EKF, HIF and AHIF algorithms can predict the SOC value more accurately, but through the improvement of the covariance matrix, the AHIF algorithm has a stronger tracking effect and more accurate estimation ability, as can be seen from the error comparison chart, the AHIF algorithm also has a better stability.

4 Conclusions

The high-precision model parameter identification and the accurate estimation method of SOC provide a guarantee for the normal operation of the BMS. To improve the accuracy of model identification and the stability of estimation methods, IPSO-FFRLS and AHIF algorithms are proposed to estimate SOC. A second-order Thevenin model is established to verify the algorithm under three different working conditions. Experimental results show that the improvement of the inertia weight ω in PSO algorithm can effectively improve the accuracy and convergence speed, the IPSO algorithm can select the optimal forgetting factor in FFRLS and IPSO-FFRLS algorithm has higher parameter identification accuracy than fixed forgetting factor FFRLS algorithm. The experimental results also prove that it is feasible to improve the SOC estimation accuracy by dynamically adjusting the noise covariance in HIF algorithm. The maximum absolute estimation error of the AHIF algorithm is 1.92%, 1.31% and 1.11% under HPPC, DST and BBDST conditions, respectively. The IPSO-FFRLS algorithm can obtain high-precision model parameters, thereby improving the SOC estimation effect. The AHIF algorithm can accurately estimate the SOC with good stability and can be used in complex working conditions. The combined algorithm of IPSO-FFRLS and AHIF provides a theoretical basis for lithium-ion battery state estimation, it also promotes the intelligent development of BMS, and plays a positive role in prolonging the service life and improving the safety performance of lithium-ion batteries.

The experiments of this research are carried out at room temperature, and the influence of high temperature or low temperature on SOC estimation has not been considered. In the future, experiments in different temperature ranges will be carried out on the basis of this study to further explore the estimation accuracy of IPSO-FFRLS algorithm and AHIF algorithm under different temperature conditions, to improve the practicability of the proposed algorithms.

Acknowledgments

The work is supported by the National Natural Science Foundation of China (No. 62173281, 61801407), Sichuan science and technology program (No. 2019YFG0427), China Scholarship Council (No. 201908515099), and Fund of Robot Technology Used for Special Environment Key Laboratory of Sichuan Province (No. 18kftk03).

Data Availability Statement

The data that support the findings of this study are available from the corresponding author upon reasonable request.

References

[1] Wang, K., X. Feng, J.B. Pang, et al., State of Charge (SOC) Estimation of Lithium-ion Battery Based on Adaptive Square Root Unscented Kalman Filter. International Journal of Electrochemical Science, 2020. **15**(9): p. 9499-9516.

[2] Zhao, B., J. Hu, S.P. Xu, et al., Estimation of the SOC of Energy-Storage Lithium Batteries Based on the Voltage Increment. Ieee Access, 2020. **8**: p. 198706-198713.

[3] Wadi, A., M. Abdel-Hafez, A. Hussein, et al., Alleviating Dynamic Model Uncertainty Effects for Improved Battery SOC Estimation of EVs in Highly Dynamic Environments. Ieee Transactions on Vehicular Technology, 2021. **70**(7): p. 6554-6566.

[4] Qiao, J.L., S.L. Wang, C.M. Yu, et al., A novel bias compensation recursive least square-multiple weighted dual extended Kalman filtering method for accurate state-of-charge and state-of-health co-estimation of lithium-ion batteries. International Journal of Circuit Theory and Applications, 2021. **49**(11): p. 3879-3893.

[5] Ren, H.B., Y.Z. Zhao, S.Z. Chen, et al., Design and implementation of a battery management system with active charge balance based on the SOC and SOH online estimation. Energy, 2019. **166**: p. 908-917.

[6] Oh, H., J. Jeon and S. Park, Effects of Battery Model on the Accuracy of Battery SOC Estimation Using Extended Kalman Filter under Practical Vehicle Conditions Including Parasitic Current Leakage and Diffusion Of Voltage. International Journal of Automotive Technology, 2021. **22**(5): p.

1337-1346.

[7] Zhou, S.Y., Z.Q. Chen, D.Y. Huang, et al., A Fault-Tolerant SoC Estimation Method for Series-Parallel Connected Li-Ion Battery Pack. Ieee Transactions on Power Electronics, 2021. **36**(12): p. 13434-13448.

[8] Wang, Y.C., D.W. Meng, Y.J. Chang, et al., Research on online parameter identification and SOC estimation methods of lithium-ion battery model based on a robustness analysis. International Journal of Energy Research, 2021. **45**(15): p. 21234-21253.

[9] Talha, M., F. Asghar and S.H. Kim, A Neural Network-Based Robust Online SOC and SOH Estimation for Sealed Lead-Acid Batteries in Renewable Systems. Arabian Journal for Science and Engineering, 2019. **44**(3): p. 1869-1881.

[10] Li, W.Q., Y. Yang, D.Q. Wang, et al., The multi-innovation extended Kalman filter algorithm for battery SOC estimation. Ionics, 2020. **26**(12): p. 6145-6156.

[11] Li, S., K. Li, E. Xiao, et al., Joint SoC and SoH Estimation for Zinc-Nickel Single-Flow Batteries. Ieee Transactions on Industrial Electronics, 2020. **67**(10): p. 8484-8494.

[12] Roselyn, J.P., A. Ravi, D. Devaraj, et al., Optimal SoC Estimation Considering Hysteresis Effect for Effective Battery Management in Shipboard Batteries. Ieee Journal of Emerging and Selected Topics in Power Electronics, 2021. **9**(5): p. 5533-5541.

[13] Li, J.B., M. Ye, K.P. Gao, et al., SOC estimation for lithium-ion batteries based on a novel model. Iet Power Electronics, 2021. **14**(13): p. 2249-2259.

[14] Ouyang, Q., J. Chen, J. Zheng, et al., SOC Estimation-Based Quasi-Sliding Mode Control for Cell Balancing in Lithium-Ion Battery Packs. Ieee Transactions on Industrial Electronics, 2018. **65**(4): p. 3427-3436.

[15] Wang, Y., J. Tian, Z. Sun, et al., A comprehensive review of battery modeling and state estimation approaches for advanced battery management systems. Renewable and Sustainable Energy Reviews, 2020. **131**: p. 110015.

[16] Ipek, E. and M. Yilmaz, A novel method for SOC estimation of Li-ion batteries using a hybrid machine learning technique. Turkish Journal of Electrical Engineering and Computer Sciences, 2021. **29**(1): p. 18-31.

[17] Han, W.J., C.F. Zou, C. Zhou, et al., Estimation of Cell SOC Evolution and System Performance in Module-Based Battery Charge Equalization Systems. Ieee Transactions on Smart Grid, 2019. **10**(5): p. 4717-4728.

[18] Hannan, M.A., D.N.T. How, M.S.H. Lipu, et al., SOC Estimation of Li-ion Batteries With Learning Rate-Optimized Deep Fully Convolutional Network. Ieee Transactions on Power Electronics, 2021. **36**(7): p. 7349-7353.

[19] Xu, X., Y.Z. Lin, F. Wang, et al., A hybrid observer for SOC estimation of lithium-ion battery based on a coupled electrochemical-thermal model. International Journal of Green Energy, 2019. **16**(15): p. 1527-1538.

[20] Li, Y., B.Y. Xiong, D.M. Vilathgamuwa, et al., Constrained Ensemble Kalman Filter for Distributed Electrochemical State Estimation of Lithium-Ion Batteries. Ieee Transactions on Industrial Informatics, 2021. **17**(1): p. 240-250.

[21] Xu, W.H., S.L. Wang, C. Jiang, et al., A novel adaptive dual extended Kalman filtering algorithm for the Li-ion battery state of charge and state of health co-estimation. International Journal of Energy Research, 2021. **45**(10): p. 14592-14602.

[22] Cen, Z.H. and P. Kubiak, Lithium-ion battery SOC/SOH adaptive estimation via simplified single particle model. International Journal of Energy Research, 2020. **44**(15): p. 12444-12459.

[23] Wang, Y.J. and Z.H. Chen, A framework for state-of-charge and remaining discharge time prediction using unscented particle filter. Applied Energy, 2020. **260**.

[24] Li, J.B., M. Ye, K.P. Gao, et al., State estimation of lithium polymer battery based on Kalman filter. Ionics, 2021. **27**(9): p. 3909-3918.

[25] Chen, Y., C.L. Li, S.Z. Chen, et al., A combined robust approach based on auto-regressive long short-term memory network and moving horizon estimation for state-of-charge estimation of lithium-ion batteries. International Journal of Energy Research, 2021. **45**(9): p. 12838-12853.

[26] Duan, W.X., C.X. Song, Y. Chen, et al., Online Parameter Identification and State of Charge Estimation of Battery Based on Multitimescale Adaptive Double Kalman Filter Algorithm. Mathematical Problems in Engineering, 2020. **2020**.

[27] Yang, F.F., S.H. Zhang, W.H. Li, et al., State-of-charge estimation of lithium-ion batteries using LSTM and UKF. Energy, 2020. **201**.

[28] Wang, Y., R. Xu, C. Zhou, et al., Digital twin and cloud-side-end collaboration for intelligent battery management system. Journal of Manufacturing Systems, 2022. **62**: p. 124-134.

[29] Hu, L., X.S. Hu, Y.H. Che, et al., Reliable state of charge estimation of battery packs using fuzzy adaptive federated filtering. Applied Energy, 2020. **262**.

[30] Wang, Y.J., L. Wang, M.C. Li, et al., A review of key issues for control and management in battery and ultra-capacitor hybrid energy storage systems. Etransportation, 2020. **4**.

[31] Lin, Y.Z., X. Xu, F. Wang, et al., Active equalization control strategy of Li-ion battery based on state of charge estimation of an electrochemical-thermal coupling model. International Journal of Energy Research, 2020. **44**(5): p. 3778-3789.

[32] Li, H.H., X.Y. Wang, A. Saini, et al., State of Charge Estimation for Lithium-Ion Battery Models Based on a Thermoelectric Coupling Model. International Journal of Electrochemical Science, 2020. **15**(5): p. 3807-3824.

[33] Xu, W.H., S.L. Wang, C. Fernandez, et al., Novel reduced-order modeling method combined with three-particle nonlinear transform unscented Kalman filtering for the battery state-of-charge estimation. Journal of Power Electronics, 2020. **20**(6): p. 1541-1549.

[34] Fang, Y.Y., Q. Zhang, H. Zhang, et al., State-of-charge estimation technique for lithium-ion batteries by means of second-order extended Kalman filter and equivalent circuit model: Great temperature robustness state-of-charge estimation. Iet Power Electronics, 2021. **14**(8): p. 1515-1528.

[35] Zhang, C., W. Allafi, Q. Dinh, et al., Online estimation of battery equivalent circuit model parameters and state of charge using decoupled least squares technique. Energy, 2018. **142**: p. 678-688.

[36] Ren, Z., C.Q. Du, Z.Y. Wu, et al., A comparative study of the influence of different open circuit voltage tests on model-based state of charge estimation for lithium-ion batteries. International Journal of Energy Research, 2021. **45**(9): p. 13692-13711.

[37] Zhao, L.H., Z.Y. Liu and G.H. Ji, Lithium-ion battery state of charge estimation with model parameters adaptation using H-infinity, extended Kalman filter. Control Engineering Practice, 2018. **81**: p. 114-128.

[38] Chen, C., R. Xiong and W.X. Shen, A Lithium-Ion Battery-in-the-Loop Approach to Test and Validate Multiscale Dual H Infinity Filters for State-of-Charge and Capacity Estimation. Ieee Transactions on Power Electronics, 2018. **33**(1): p. 332-342.